IEEE Access
Multidisciplinary | Rapid Review | Open Access Journal

Received February 12, 2022, accepted March 11, 2022, date of publication March 21, 2022, date of current version March 30, 2022.

Digital Object Identifier 10.1109/ACCESS.2022.3160885

Ultralow RF Signal Loss in Aerosol Jet Printed Silver Microstrip Lines up to 18 GHz

EVA S. ROSKER[1,2], MICHAEL T. BARAKO[1], TAN TRAN[1], EVAN NGUYEN[1], MARK S. GOORSKY[2], AND JESSE TICE[1]

[1]Northrop Grumman Corporation, Redondo Beach, CA 90278, USA
[2]Department of Materials Science and Engineering, UCLA, Los Angeles, CA 90024, USA

Corresponding author: Eva S. Rosker (erosker@ucla.edu)

ABSTRACT Printed radio frequency (RF) electronic components are often prohibitively lossy due to the materials challenges involved in additively manufacturing metals and dielectrics. We use aerosol jet printing of reactive silver inks to fabricate microstrip transmission lines onto commercial RF boards and subsequently extract the insertion loss of the printed silver through bisect de-embedding of the transmission lines. We directly compare the performance of our printed silver microstrips to conventional copper-clad microstrips to benchmark the efficacy of additive manufacturing against traditional processing methods. With an insertion loss nearing that of conventional copper, reactive silver ink printed traces offer dense continuous metals that can reliably act as conductors for RF applications. In addition to the morphological effects on loss from the printed metal itself, we also observe that the effect of substrate surface texture contributes to unexpected loss that may be mitigated by smoothing the surface or aligning the print direction to minimize these effects. Metallizing passive RF components using reactive inks offers a practical approach which will allow RF designers to take advantage of three-dimensional space. This is possible without sacrificing the necessary high conductivity and low loss needed to produce high performance devices for use within aerospace and communications.

INDEX TERMS 3D printing, additive manufacturing, microstrip line, printed circuit board.

I. INTRODUCTION

Additive manufacturing (AM) has rapidly expanded three-dimensional design space to enable radio frequency (RF) device designs that cannot be produced using conventional manufacturing. This additional degree of processing freedom has been used to additively manufacture a diverse array of RF structures from simple transmission lines [1]–[3], waveguides [4], [5], and patch antennas [6]–[8] to more complex three-dimensional RF filters [9]–[11] and antennas exhibiting unique characteristics [12]–[16] that cannot be achieved in planar configurations alone. Compared to conventional techniques, in which the signal and ground metal must be rolled-on or electrodeposited and subsequently etched, AM uses direct metal deposition to pattern features in a single step. Besides being significantly faster and more efficient than traditional processing, AM is also crucial to the manufacture of structures that are not compatible with conventional methods, such as flexible or curved components. AM methods encompass a variety of techniques, but inkjet printing and aerosol jet printing are the most common forms of direct metal deposition. However, most printable metals used for conductive traces are typically nanoparticle inks that must be sintered to form porous monoliths, and exhibit poor transport properties due to microstructural defects and tortuosity, grain boundaries, impurities, and topological surface roughness [17]–[20]. For DC and low frequency operation, these defects manifest as a reduction in the effective conductivity and increase the Ohmic losses of current carrying traces. As the operating frequencies increase into the RF bands, the parasitic impedances induced by reflection at interfaces, increased scattering from rough surfaces, and the morphological tortuosity that interrupts wave propagation combine to inhibit electronic conduction in nanoparticle-based traces that is difficult to replicate and can be orders of magnitude below plated metals and other conventionally fabricated RF circuits [21]. This deficiency in material properties has relegated many additive

The associate editor coordinating the review of this manuscript and approving it for publication was Pedro Neto.

manufacturing efforts to rapid prototyping applications, particularly when operating in the RF regime, where the benefits of three-dimensional architectures are negated by the significant degradation in material properties compared to their conventional counterparts. Recently, Cai *et al.* [22] have characterized the insertion loss of printed nanoparticle inks at frequencies as high as 40 GHz. This demonstration underlies the immense potential for printed metals systems within RF, but represents only one part of the toolbox of materials available to designers and engineers. An alternate to nanoparticle inks comes in the form of reactive metal inks, which have been developed in large part to mitigate many of the fundamental materials challenges inherent to particle-based compositions[23]–[30]. This is achieved by producing solid, interface-free metals with densities approaching unity and DC conductivities that can exceed 70% of the bulk metal value. We have previously shown near-bulk DC conductivity using reactive metal inks and have furthermore shown that these traces are capable of carrying RF signals [31]. Here we investigate the use of one method of additive manufacturing, aerosol jet printing, to print RF signal traces and measure the transmission and insertion losses of reactive metal microstrips on conventional RF substrates. By exploring the intersection of an emerging materials system with a novel processing technique, we seek to provide a broader understanding of signal conduction in printed metals. The dense metals resulting from reactive inks reduce the number of scattering sites and other impediments that would otherwise produce prohibitively large insertion losses, and provide a viable means towards achieving fully 3D printed microwave passive circuit elements that show no deviation from conventional metals yet retain the benefits of 3D fabrication.

II. DEVICE FABRICATION AND TESTING

We use a reactive silver ink to print RF microstrip transmission lines on a conventional circuit board substrate – FR4 laminate (thickness t = 0.5mm, dielectric constant $\varepsilon_r = 4.3$) – as shown in **Fig. 1**. Two copies of each microstrip are produced to directly compare the RF properties of metals fabricated via conventional processing against the more novel AM approach. In each set, one device under test (DUT) is entirely fabricated using conventional chemical etching of copper cladding as a representative baseline. The second DUT in each set has only the launches, connector feeds, and ground planes fabricated from patterned copper cladding such that the signal traces connecting the two launches can be aerosol jet-printed with reactive silver. This design ensures that the reference plane for our measurement is at the edge of the printed silver trace, thereby ensuring that only the printed area will be under test in a side-by-side comparison to copper cladding.

The silver DUTs are printed using our previously-published protocol [31][32]. In brief, a reactive silver ink (Electroninks EI-1403) is aerosolized using an Optomec AJ300 aerosol jet printer fitted with a 100 μm nozzle. The substrate is held at 80°C which causes the printed ink to undergo a low-temperature heat treatment, thereby solidifying the liquid ink into a dense continuous metal film [33]. The signal traces are printed in 10 passes, which results in a metal thickness of approximately 3 μm, to ensure that our measurements do not reflect any irregular behavior arising from the skin depth effect, which for the lowest frequency of 2 GHz is estimated to be only 1.4 μm.

We measure the devices at radio frequencies by testing all microstrips using a portable network analyzer (PNA) from 20 MHz to 20 GHz with a two-port configuration. We focus on the frequency range 2-18 GHz, which encompasses the S (2-4 GHz), C (4-8 GHz), X (8-12 GHz), and K_u (12-18 GHz) bands, as these bands are highly utilized across a variety of applications including telecommunications, radar, satellite communications, and WiFi. The PNA cables are calibrated using a standard Short-Open-Load-Through (SOLT) calibration toolkit, in which we isolate the insertion loss of the transmission line segment by removing contributions from the launch, connectors, and cables. We extract the insertion loss of the metal conductor using the two-line THRU and LINE standard method with microstrips of different lengths (6 inch, 8 inch, and 10 inch). While this method requires only one pair of microstrips, we print three different lengths to ensure that we have multiple DUTs available for the extraction. After collecting the S-parameter data, we use CST Microwave Studio to model the expected behavior from known device design parameters and to extract the insertion loss and complex permittivity from the measured data. The complex permittivity encompasses the real component of the substrate dielectric constant as well as the loss tangent, and we compare these extracted values against the known data sheet values to validate the fit of our insertion loss simulation.

The board material also has an effect on the overall loss present in the RF structure. FR4 is a relatively lossy substrate ($\tan\delta = 0.025$), so we also print similar DUTs onto a lower-loss circuit board material, Taconic TLX-9 (thickness t = 0.25 mm, dielectric constant $\varepsilon_r = 2.5$, $\tan\delta = 0.0019$ [34]), to demonstrate the utility of this technique for high performance circuit components. This material is a woven PTFE composite that also presents unique challenges regarding the nonuniform surface finish, as discussed in the subsequent sections.

III. RESULTS AND DISCUSSION

A. FR4 BOARD

The measured S-parameter reflection (S11) and transmission (S12) characteristics are presented in **Fig. 2**. Comparing the printed silver traces to the conventional etched copper, we observe an identical and consistent slope offset of roughly 0.2 dB/GHz between each silver vs copper device length pair. This offset corresponds to a discrepancy in the raw measured data that includes contributions from fixturing effects. We also observe similar rippling in each length pair

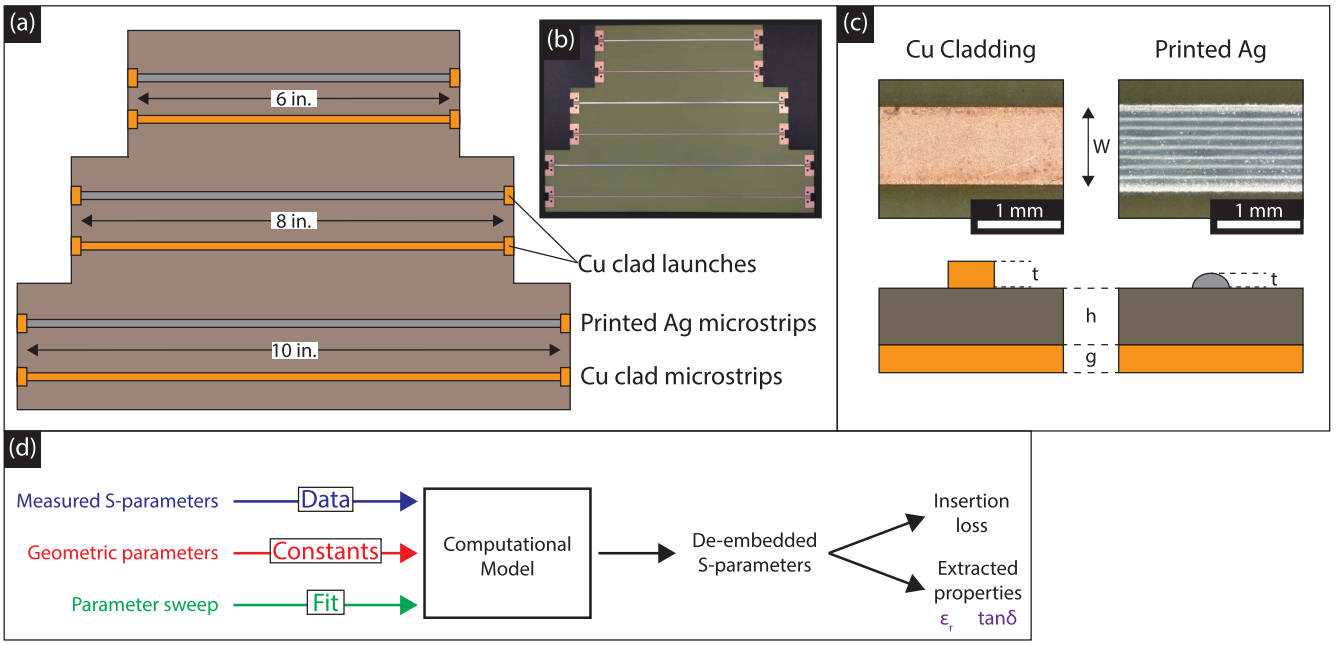

FIGURE 1. Board design, dimensions, and model approach used in this study. (a) Schematic and (b) photograph of microstrip elements on FR4 substrate, showing the three pairs of copper cladding and printed silver microstrips. (c) Microscope images of the copper clad and printed silver traces. The silver microstrips are created by overlapping adjacent sub-traces until the desired microstrip width is achieved. (d) The data reduction scheme uses a computational model to extract the unknown properties of the board, including the insertion loss and complex permittivity components.

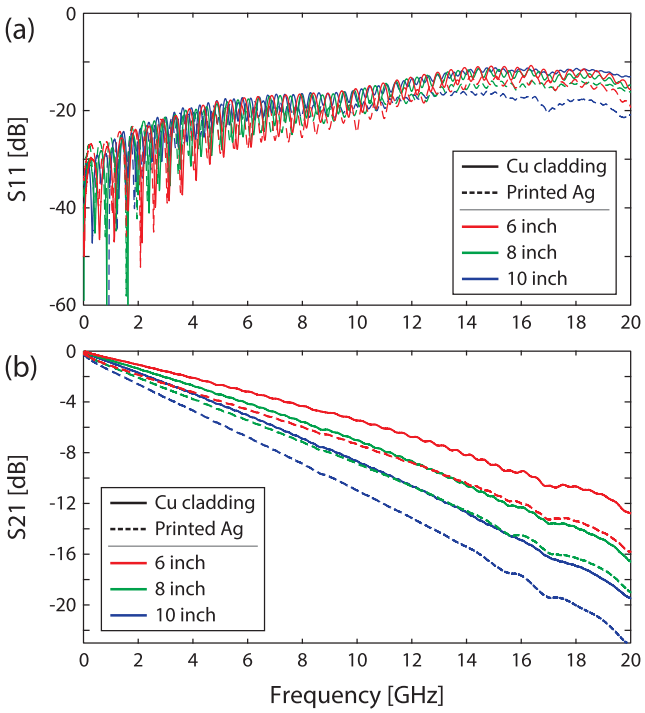

FIGURE 2. Measured RF S-parameter data of the FR4 board DUTs. S11 is the reflection and S12 is the transmission behavior of the microstrips. For each set of microstrip lengths, the printed silver exhibits a 0.2 dB/GHz slope offset compared to the etched copper for the raw measured signal, which includes fixturing effects.

of silver vs copper DUTs. This behavior originates from a combination of the inherently lossy substrate material as well as the fixturing effects. Since there is a uniform shift across each pair of S21 curves, we conclude that the printed silver itself is not introducing any more loss than the copper and is in fact behaving exactly as a conventional metal would. To remove fixturing effects and extract the inherent insertion loss of each metal, we use the two-line method to extrapolate the insertion loss from two microstrip transmission lines of known length. We use THRU bisect de-embedding [35], [36] to remove any signal beyond the reference plane and ensure that we are isolating the contribution from the printed silver from edge effects at the launches and connectors. The bisect de-embedding method makes use of transmission line mathematics to divide a two-port THRU line into mirrored halves. The mirrored portions can then be eliminated from each port, thereby returning only the transmission properties of the embedded DUT. By measuring at least two lengths of the same material, we can de-embed the transmission line properties. We use CST Microwave Studio to extract the complex permittivity from the measured and simulated S-parameters by comparing the data against known properties such as the substrate dielectric constant and loss tangent. The use of CST Microwave Studio is necessary to model our printed silver DUTs, as the dissimilar ground and top plane metals require 3D electromagnetic simulation. Lower complexity RF tools and analytical models would not be able to properly capture the physical effects of our DUT. The model takes in the measured S-parameter data and the fixed geometric device parameters listed in **Table 1** and uses a 3D finite element approach to simulate the behavior of the fundamental line structure, i.e. the two-inch difference in length between the THRU and LINE microstrips. The extracted

TABLE 1. Board properties and device dimensions.

Quantity	FR4	TLX-9
Dielectric constant, ε_r	4.3	2.5
Loss tangent, δ	0.025	0.0019
Board thickness, **h** [mm]	0.5	0.25
Microstrip width, **w** [mm]	1.0	0.76
Cu microstrip thickness, **t** [μm]	35.6	35.6
Ag microstrip thickness, **t** [μm]	3.0	3.0, 6.0
Ground thickness, **g** [μm]	35.6	35.6
Microstrip lengths, **L** [mm]	152, 203, 354	152, 203, 254
Cu microstrip roughness [μm]	1.54	1.54
Ground roughness [μm]	1.54	1.54
Cu conductivity [S/m]	5.8×10^7	5.8×10^7

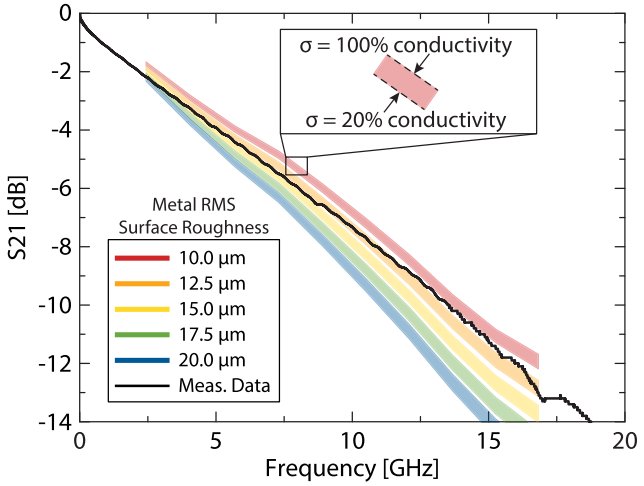

FIGURE 3. CST Studio parameter sweep plotted against measured 6 inch silver microstrip S12 data. The surface roughness and conductivity were varied in the model in order to produce the colored curves. Each band corresponds to a discrete surface roughness value and is bounded by the relative conductivity percentages. The bottom bound of each band is 20% bulk silver conductivity, while the top bound is 100%.

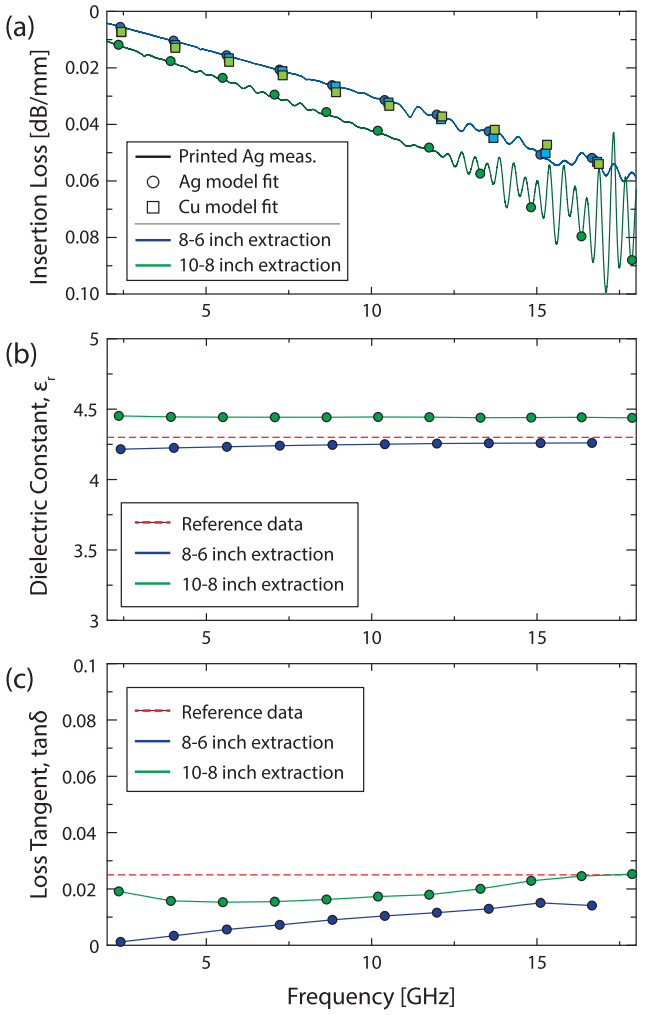

FIGURE 4. Properties extracted from the CST Studio simulation. The FR4 substrate dielectric constant and loss tangent are simulated across the frequency band and fitted against the known properties from the dielectric substrate data sheet. The resulting fit takes into account these properties and returns the material insertion loss across frequencies.

dielectric constant and loss tangent of the substrate are compared to the known data sheet values to assess the quality of the fit.

Additionally, we perform a parameter sweep of the unknown variables (microstrip conductivity and surface roughness) in our simulation and plot the results against the measured 6 inch microstrip data. This is done to ensure that the resulting model fit is representative of realistic device properties. **Fig. 3** shows the 6 inch silver microstrip data overlaid on top of colored bands created by performing the simulation with different microstrip conductivities and surface roughness values. From this parameter sweep, we observe that the measured data cleanly lines up within the band corresponding to 15 ± 2.5 μm (0.6 ± 0.1 mil) root mean square surface roughness. The measured data is not confined to one particular conductivity percentage in this band, indicating that at radio frequencies the printed metal system is heavily dominated by losses due to surface effects moreso than the inherent conductivity of the metal. While it may be possible to deconvolute these two parameters [37], the practical applications of this finding suggest that we can reasonably assume our printed silver to show effectively no deviation from a conventional bulk metal strictly in terms of conductivity up to 18 GHz. This has exciting implications for RF electronics processing, as this method of fabrication presents a viable means to realize complex device architectures that perform at the level expected from conventional metallization. By assuming a surface roughness of 15 μm along with a conductivity of 100% bulk silver into the model, we see a nearly-overlapping fit for both pairs of microstrips (i.e. 6 and 8 inch, and 8 and 10 inch).

The simulation output is shown in **Fig. 4**, where we plot the insertion loss of the fundamental 2 inch de-embedded structure as a function of frequency as well as the extracted

dielectric constant, ε_r, and loss tangent, tanδ. Across the entire frequency range tested, the dielectric constant extracted from the simulation is at most 3% different than the known data sheet value of 4.3, indicating that we have reached good agreement between the model and our physical DUT. Similarly, the extracted dielectric loss tanδ is reasonably close to the known value of 0.025. The extracted loss tangent deviates from the reference data to a greater extent at lower frequencies, and this is because the length of the traces may be too short to accurately account for dielectric losses. Since attenuation is reduced at lower frequencies, we are therefore more sensitive to measurement noise at lower frequencies and may be close to the measurement error floor. Notably, we observe that the model fit for a 2 inch microstrip is clearly aligned to the extracted 2 inch difference between the THRU and LINE data that was measured. This figure therefore displays the insertion loss in decibels per unit length of our printed reactive silver at any frequency between 2-18 GHz. At 10 GHz, the insertion loss is 0.038 $\pm$ 0.007 dB/mm (0.96 $\pm$ 0.2 dB/inch). The slight discrepancy between the two silver extractions can be explained by the positioning of the printed silver traces over the copper launches. Since the precise physical alignment of the traces was not identical, this results in two slightly different ripple patterns in each measured S21 curve. This minor difference in ripple behavior is what causes each extraction to have a marginally different extracted value. However we observe that both slopes are the same, which indicates that this offset is not a feature of the printed trace itself beyond the fixturing effects. One other thing to note is that the oscillatory effect observed at high frequencies in the 10-8 inch extraction is due to the differences between the S21 data for each microstrip. The additional loss in the 10 inch line results in a less pronounced ripple effect than in the 8 inch data, and this mismatch during the extraction manifests in the behavior observed here. This could potentially be smoothed by performing time domain gating on the data.

Performing the insertion loss extraction on the copper clad data set yields an identical amount of loss across frequencies to that observed in the printed silver data set. The de-embedding process removes any loss contributions outside of the center portion of the trace, which means that the inherent insertion loss within the printed silver trace is equal with conventional copper cladding. Plotting the unwrapped phase of each microstrip pair validates that the lengths are identical, so the excess loss observed in the raw data must exclusively be a result of the test fixture. This can come from several factors. First, any geometric effects arising from dissimilar top and ground plane metals can increase the loss observed in the DUT by a small amount. Second, the inhomogeneity of the launch interface (i.e. the abrupt transition from copper cladding to printed silver) results in a scattering site that manifests as an offset loss which is consistent for each DUT length pair. This could be mitigated by improving the transition design to reduce the loss added as a result of the test fixture. This could also be addressed by using a TRL calibration which would place the reference planes inside the copper launches.

TABLE 2. Summary of key reported insertion loss values.

Reference	Insertion Loss [dB/mm]	Freq. [GHz]	Structure	Metallization
[2]	0.2	18	CPW	Printed Silver
[3]	0.3	18	Microstrip	Printed Silver
[15]	0.25	10	Microstrip	Printed Silver
[22]	0.20	10	Stripline	Printed Silver
[38]	0.033	10	Microstrip	Etched Copper
This Work	**0.038**	**10**	**Microstrip**	**Printed Silver**

B. TACONIC TLX-9 BOARD

In addition to printing on a standard RF circuit board, we also print similar DUTs onto a much lower loss RF substrate. While FR4 is a smooth laminate with a uniform and flat top surface, TLX-9 is composed of woven fibers that manifest in distinct peaks and valleys across the circuit board. Because of this weave pattern, we observe greatly exaggerated loss originating from the substrate texturing in addition to the inherent conductor loss originating from the morphology of the printed metal. A typical metal should exhibit behavior in which the microstrip loss scales proportionately with line length. However, for the printed silver microstrips on the TLX-9 board, we did not observe this phenomenon. In fact, as shown in **Fig. 5**, the 10 inch microstrip had the lowest loss of the three. Notably, the etched copper cladding microstrips on this board did not display this behavior, which indicates that this phenomenon is representative of morphological effects present only in the silver traces that arise from the challenging surface texture of the board.

The woven texture of the TLX9 board is observed to have a distinct impact on the morphology of the printed line, including the introduction of line edge roughness and undulation in thickness, which collectively vary with the spatial frequency of the weave. Due to this texture, the 6 inch and 8 inch lines each exhibit notable periodic features across the length of the trace. These features line up with the texture of the board (see **Fig. 6**) and suggest that the weave pattern of the board is causing the ink to well up in certain regions and shear in others during printing. After solidification, the resulting metal contains edge defects as well as areas of varying thickness. This periodic change in metal thickness combined with the nonuniformity of the printed trace should understandably increase the number of scattering sites along the trace and could contribute to the inverted loss behavior that was observed. Notably, these features were not seen on the FR4 board, which is a more homogeneous substrate. While the printed traces are still capable of carrying RF signal, it is clear that surface texturing poses a significant challenge to achieving interface-free

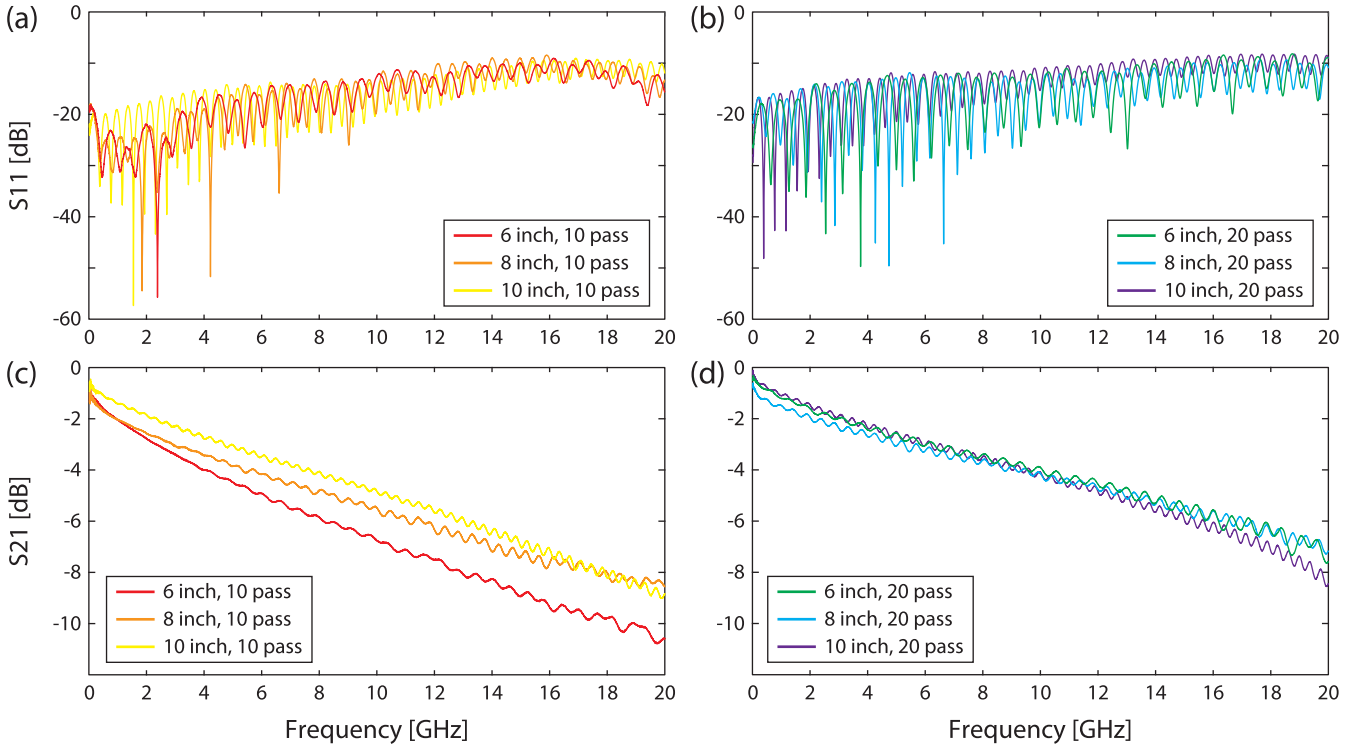

FIGURE 5. Effects of metal thickness on RF signal attenuation for TLX9 board. With only 10 passes (3 μm), there is inverted loss in which the loss increases as the microstrips get shorter. However, printing an additional 10 passes begins to negate some of the surface effects contributing to irregular behavior. At 20 passes (6 μm), the loss is approximately equal for all three microstrips and the overall loss is lower than the 10-pass data.

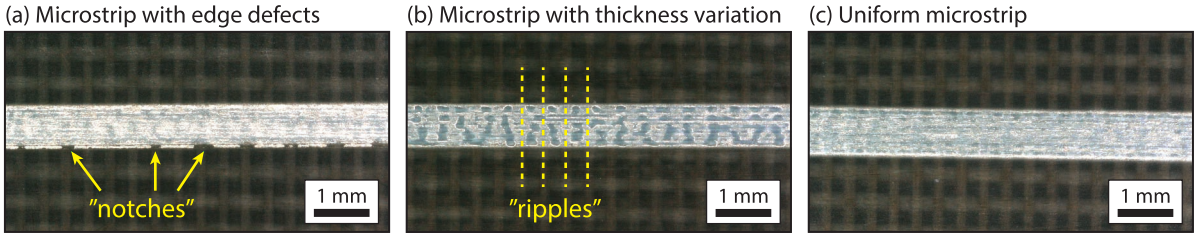

FIGURE 6. Microscope images of surface irregularities of the initial 3 μm-thick TLX-9 silver prints. Features such as "notches" (left) in the 6 inch trace and "ripples" (center) in the 8 inch trace line up with the weave pattern of the board, indicating that the surface may need to be modified in order to see smoother prints. The rightmost image shows the more uniform 10 inch printed trace with clean, sharp edges and a smooth top surface.

printed metals that perform at a level commensurate to those printed on flatter substrates. The 10 inch line shows the most uniform morphology and exhibits the lowest loss overall, while the 6 and 8 inch microstrips each contain defects (notches and ripples, respectively) that inhibit the signal carrying capacity of the trace and manifest in high attenuation due to conductor losses. The print process for each microstrip was identical, but it was likely their positioning on the weave pattern of the board that caused these defects.

Due to this unexpected loss behavior, we also evaluate the role of metal thickness, as determined by the total number of printing passes, on the RF transmission properties. We use the same Taconic TLX-9 board as before and add an additional 10 passes ($\sim$3 μm, for a total thickness of $\sim$6 μm) of printed silver onto the existing traces and remeasure the S-parameters. By printing thicker metal, we attempt to increase the uniformity of the trace by planarizing the periodic effects present in the first set of microstrips. After adding the additional silver layers, all DUTs exhibited approximately the same amount of loss (see **Fig. 5**) despite being three different lengths and consisting of different morphologies. While this is still atypical behavior for metal microstrips, the change in relative performance indicates that it may be possible to overcome the role of the substrate surface by introducing additional thickness into the printed line. In this case, the additional metal thickness was not enough to fully overcome the periodic perturbations originating from the textured board, but it does appear that by printing thicker we

are able to mitigate some of these effects. For nonuniform substrates, it will therefore be necessary to build up enough thickness to properly conformally-coat the surface and avoid any unintended scattering centers along the length of the metallized part. RF performance in additively manufactured devices does depend on material quality for transport, but there is also a significant contribution from the surface properties. As new processes emerge for manufacturing printed substrates, consideration must be given to their surface finish and texturing for successful integration with printed metals. This will become an area of great importance as the field of printed RF electronics moves toward newer and more interesting substrate materials.

IV. CONCLUSION

This work represents a critical path forward in moving additive manufacturing out of the rapid prototyping niche and into scaled manufacturing of high-performance RF devices. By illuminating the fundamental material requirements and identifying that surface roughness presents a key barrier to high conductivity printed metals, we show that RF elements can be printed with comparable performance to conventionally manufactured boards. As RF designers begin to move into the three-dimensional design space, this approach can now be used to realize new additively manufactured RF architectures that retain conventional material properties but enable unique device performance that is unattainable by planar processes. A similar approach is now required for printable low-loss dielectric materials which, when combined with reactive metal inks, can be used in high-performance, fully-additively manufactured RF electronics.

REFERENCES

[1] M. Abt, A. Roch, J. A. Qayyum, S. Pestotnik, L. Stepien, A. Abu-Ageel, B. Wright, A. C. Ulusoy, J. Albrecht, L. Harle, J. Papapolymerou, and T. Schuelke, "Aerosol-printed highly conductive ag transmission lines for flexible electronic devices," *IEEE Trans. Compon., Packag., Manuf. Technol.*, vol. 8, no. 10, pp. 1838–1844, Oct. 2018.

[2] T. Shimizu and Y. Kogami, "Microwave characteristics of a conductor backed CPW by a home printed electronics technology with silver nanoparticle ink," in *Proc. Asia–Pacific Microw. Conf. (APMC)*, Nov. 2018, pp. 1229–1231.

[3] A. A. Gupta, M. C. M. Soer, M. Taherzadeh-Sani, S. G. Cloutier, and R. Izquierdo, "Aerosol-jet printed transmission lines for microwave packaging applications," *IEEE Trans. Compon., Packag., Manuf. Technol.*, vol. 9, no. 12, pp. 2482–2489, Dec. 2019.

[4] L. D. van Putten, J. Gorecki, E. N. Fokoua, V. Apostolopoulos, and F. Poletti, "3D-printed polymer antiresonant waveguides for short-reach terahertz applications," *Appl. Opt.*, vol. 57, no. 14, p. 3953, 2018.

[5] Y. Kim, Y. Cui, M. M. Tentzeris, and S. Lim, "Additively manufactured electromagnetic based planar pressure sensor using substrate integrated waveguide technology," *Additive Manuf.*, vol. 34, Aug. 2020, Art. no. 101225.

[6] U. Hasni, R. Green, A. V. Filippas, and E. Topsakal, "One-step 3D-printing process for microwave patch antenna via conductive and dielectric filaments," *Microw. Opt. Technol. Lett.*, vol. 61, no. 3, pp. 734–740, Mar. 2019.

[7] S. Wang, L. Zhu, J. Wang, and W. Wu, "Circularly polarised patch antenna using 3D-printed asymmetric substrate," *Electron. Lett.*, vol. 54, no. 11, pp. 674–676, May 2018.

[8] Y. Zhou, S. Sivapurapu, R. Chen, N. A. Amoli, M. Bellaredj, M. Swaminathan, and S. K. Sitaraman, "Study of electrical and mechanical characteristics of inkjet-printed patch antenna under uniaxial and biaxial bending," in *Proc. IEEE 69th Electron. Compon. Technol. Conf. (ECTC)*, May 2019, pp. 1939–1945.

[9] Y. Zhang, F. Zhang, Y. Gao, J. Xu, C. Guo, and X. Shang, "3D printed waveguide step-twist with bandpass filtering functionality," *Electron. Lett.*, vol. 56, no. 11, pp. 527–528, 2020.

[10] M. Sippel, K. Lomakin, M. Ankenbrand, M. Petersen, J. Franke, K. Helmreich, M. Vossiek, and G. Gold, "3D-printed bowtie filter created by high precision NanoJet system combined with novel printing strategy," in *Proc. IEEE 28th Conf. Electr. Perform. Electron. Packag. Syst. (EPEPS)*, Oct. 2019, pp. 5–7.

[11] M. Ortiz-Martinez, E. Castro-Camus, and A. I. Hernandez-Serrano, "Guided-mode filters for terahertz frequencies fabricated by 3D printing," *J. Infr., Millim., THz Waves*, vol. 40, no. 7, pp. 731–737, Jul. 2019.

[12] M. W. Sabri, N. A. Murad, and M. K. A. Rahim, "Highly directive 3D-printed dual-beam waveguide slotted antennas for millimeter-wave applications," *Microw. Opt. Technol. Lett.*, vol. 61, no. 6, pp. 1566–1573, Jun. 2019.

[13] M. A. Belen, "Stacked microstrip patch antenna design for ISM band applications with 3D-printing technology," *Microw. Opt. Technol. Lett.*, vol. 61, no. 3, pp. 709–712, Mar. 2019.

[14] P. Parthiban, B. Seet, and X. J. Li, "3D-printed circularly polarized concave patch with enhanced bandwidth and radiation pattern," *Microw. Opt. Technol. Lett.*, vol. 63, no. 2, pp. 572–580, Feb. 2021.

[15] I. Piekarz, J. Sorocki, M. T. Craton, K. Wincza, S. Gruszczynski, and J. Papapolymerou, "Application of aerosol jet 3-D printing with conductive and nonconductive inks for manufacturing mm-wave circuits," *IEEE Trans. Compon., Packag., Manuf. Technol.*, vol. 9, no. 3, pp. 586–595, Mar. 2019.

[16] G. Muntoni, G. Montisci, G. A. Casula, F. P. Chietera, A. Michel, R. Colella, L. Catarinucci, and G. Mazzarella, "A curved 3-D printed microstrip patch antenna layout for bandwidth enhancement and size reduction," *IEEE Antennas Wireless Propag. Lett.*, vol. 19, no. 7, pp. 1118–1122, Jul. 2020.

[17] E. S. Rosker, R. Sandhu, J. Hester, M. S. Goorsky, and J. Tice, "Printable materials for the realization of high performance RF components: Challenges and opportunities," *Int. J. Antennas Propag.*, vol. 2018, Jan. 2018, Art. no. 9359528.

[18] S. K. Volkman, S. Yin, T. Bakhishev, K. Puntambekar, V. Subramanian, and M. F. Toney, "Mechanistic studies on sintering of silver nanoparticles," *Chem. Mater.*, vol. 23, no. 20, pp. 4634–4640, Oct. 2011.

[19] W. Shen, X. Zhang, Q. Huang, Q. Xu, and W. Song, "Preparation of solid silver nanoparticles for inkjet printed flexible electronics with high conductivity," *Nanoscale*, vol. 6, no. 3, pp. 1622–1628, 2014.

[20] J. Vaithilingam, E. Saleh, L. Körner, R. D. Wildman, R. J. M. Hague, R. K. Leach, and C. J. Tuck, "3-dimensional inkjet printing of macro structures from silver nanoparticles," *Mater. Design*, vol. 139, pp. 81–88, Feb. 2018.

[21] T. Björninen, S. Merilampi, L. Ukkonen, P. Ruuskanen, and L. Sydänheimo, "Performance comparison of silver ink and copper conductors for microwave applications," *IET Microw., Antennas Propag.*, vol. 4, no. 9, pp. 1224–1231, Sep. 2010.

[22] F. Cai, Y.-H. Chang, K. Wang, C. Zhang, B. Wang, and J. Papapolymerou, "Low-loss 3-D multilayer transmission lines and interconnects fabricated by additive manufacturing technologies," *IEEE Trans. Microw. Theory Techn.*, vol. 64, no. 10, pp. 3208–3216, Oct. 2016.

[23] S. B. Walker and J. A. Lewis, "Reactive silver inks for patterning high-conductivity features at mild temperatures," *J. Amer. Chem. Soc.*, vol. 134, no. 3, pp. 1419–1421, Jan. 2012.

[24] K. Black, J. Singh, D. Mehta, S. Sung, C. J. Sutcliffe, and P. R. Chalker, "Silver ink formulations for sinter-free printing of conductive films," *Sci. Rep.*, vol. 6, no. 1, pp. 1–7, Aug. 2016.

[25] Z. Zhao, A. Mamidanna, C. Lefky, O. Hildreth, and T. L. Alford, "A percolative approach to investigate electromigration failure in printed ag structures," *J. Appl. Phys.*, vol. 120, no. 12, Sep. 2016, Art. no. 125104.

[26] Y. Dong, X. Li, S. Liu, Q. Zhu, M. Zhang, J.-G. Li, and X. Sun, "Optimizing formulations of silver organic decomposition ink for producing highly-conductive features on flexible substrates: The case study of amines," *Thin Solid Films*, vol. 616, pp. 635–642, Oct. 2016.

[27] J. Kastner, T. Faury, H. M. Außerhuber, T. Obermüller, H. Leichtfried, M. J. Haslinger, E. Liftinger, J. Innerlohinger, I. Gnatiuk, D. Holzinger, and T. Lederer, "Silver-based reactive ink for inkjet-printing of conductive lines on textiles," *Microelectron. Eng.*, vol. 176, pp. 84–88, May 2017.
[28] S. F. Jahn, T. Blaudeck, R. R. Baumann, A. Jakob, P. Ecorchard, T. Rüffer, H. Lang, and P. Schmidt, "Inkjet printing of conductive silver patterns by using the first aqueous particle-free MOD ink without additional stabilizing ligands," *Chem. Mater.*, vol. 22, no. 10, pp. 3067–3071, May 2010.
[29] J.-T. Wu, S. L.-C. Hsu, M.-H. Tsai, and W.-S. Hwang, "Inkjet printing of low-temperature cured silver patterns by using $AgNO_3$/1-dimethylamino-2-propanol inks on polymer substrates," *J. Phys. Chem. C*, vol. 115, no. 22, pp. 10940–10945, Jun. 2011.
[30] Y. Chang, D.-Y. Wang, Y.-L. Tai, and Z.-G. Yang, "Preparation, characterization and reaction mechanism of a novel silver-organic conductive ink," *J. Mater. Chem.*, vol. 22, no. 48, pp. 25296–25301, 2012.
[31] E. S. Rosker, M. T. Barako, E. Nguyen, D. DiMarzio, K. Kisslinger, D.-W. Duan, R. Sandhu, M. S. Goorsky, and J. Tice, "Approaching the practical conductivity limits of aerosol jet printed silver," *ACS Appl. Mater. Interfaces*, vol. 12, pp. 29684–29691, Jun. 2020.
[32] E. S. Rosker, "Printed radio frequency electronics: Achieving high performance using additive manufacturing," Ph.D. dissertation, Univ. California, Los Angeles, CA, USA, 2021.
[33] S. Walker, "Synthesis and patterning of reactive silver inks," Ph.D. dissertation, Univ. Illinois Urbana-Champaign, Urbana-Champaign, IL, USA, 2013.
[34] *TLX High Volume Fiberglass Reinforced Microwave Substrate*, Data Sheet, Taconic, Petersburg, NY, USA, 2020.
[35] M. J. Degerstrom, B. K. Gilbert, and E. S. Daniel, "Accurate resistance, inductance, capacitance, and conductance (RLCG) from uniform transmission line measurements," in *Proc. IEEE Elect. Perform. Electron. Packag. (EPEP)*, 2008, pp. 77–80, doi: 10.1109/EPEP.2008.4675881.
[36] E. S. Daniel, N. E. Harff, V. Sokolov, S. M. Schreiber, and B. K. Gilbert, "Network analyzer measurement de-embedding utilizing a distributed transmission matrix bisection of a single THRU structure," in *Proc. ARFTG 63rd Conf. Spring*, 2004, p. 61.
[37] E. O. Hammerstad and F. Bekkadal, *A Microstrip Handbook*. Trondheim, Norway: Electronics Research Laboratory, Univ. Trondheim, 1975.
[38] X. Wu, D. Cullen, G. Brist, and O. M. Ramahi, "Surface finish effects on high-speed signal degradation," *IEEE Trans. Adv. Packag.*, vol. 31, no. 1, pp. 182–189, Feb. 2008.

EVA S. ROSKER received the Ph.D. degree in materials science and engineering from UCLA, Los Angeles, CA, USA, in 2021.

She joined the Nanomaterials Laboratory, NG Next, Northrop Grumman Corporation, Redondo Beach, CA, USA, from 2017 to 2021, and was involved with characterization of printed materials for high performance RF applications. She is currently working with the Materials and Processes Department, Northrop Grumman, to develop technologies for rapid insertion into space hardware.

MICHAEL T. BARAKO received the B.S. degree in mechanical engineering from Carnegie Mellon University, Pittsburgh, PA, USA, in 2010, and the M.S. and Ph.D. degrees in mechanical engineering from Stanford University, Stanford, CA, USA, in 2012 and 2016, respectively.

He is currently a Senior Principal Research Scientist with the Basic Research Laboratory, Northrop Grumman Corporation, Redondo Beach, CA, USA. He is the author of over 25 publications and eight patents. His research interests include emerging thermal materials and nonlinear transport physics.

Dr. Barako was a recipient of the National Defense Science and Engineering Graduate Fellowship. He has received multiple awards from IEEE for outstanding papers and presentations.

TAN TRAN received the B.S. degree in physics from the University of California at Los Angeles, Los Angeles, CA, USA, in 2008, and the M.S. degree in electrical engineering from the University of California at San Diego, San Diego, CA, USA, in 2010.

In 2010, he joined Northrop Grumman Corporation, Redondo Beach, CA, USA. He has been part of the Northrop Grumman RF Mixed Signal Products Department since 2019.

EVAN NGUYEN is a part of the Nanomaterials Laboratory, NG Next, where he focuses on material characterization and process development using additive manufacturing methods. In 2009, he joined Northrop Grumman Corporation, Redondo Beach, CA, USA, where he was with the Materials Engineering Group.

Mr. Nguyen was a recipient of the Engineering Choice Award, in 2014, for his work with additive manufacturing.

MARK S. GOORSKY received the Ph.D. degree in materials science and engineering from the Massachusetts Institute of Technology, Cambridge, MA, USA, in 1989.

Since 1991, he has been a Professor in materials science and engineering with UCLA, Los Angeles, CA, USA. He has published over 240 papers and given 180 presentations on his research and has received three U.S. patents. His research interests include materials integration and the relationship between materials defects and device performance in semiconductor structures.

JESSE TICE received the Ph.D. degree in chemistry from Arizona State University, Tempe, AZ, USA, in 2008.

He currently directs the Nanomaterials Laboratory, NG Next, Northrop Grumman Corporation, Redondo Beach, CA, USA. His research interests include molecular chemistry, synthesis, and physical characterization of nanomaterials. He is involved in nanomaterials for aerospace and defense, and has led additive manufacturing research efforts from ink development through RF performance.